Geochronology and Geochemistry of Late Devonian I- and A-Type Granites from the Xing'an Block, NE China: Implications for Slab Break-off during Subduction of the Hegenshan-Heihe Ocean

Zheng Ji[1], **Wenchun Ge**[*1], **Hao Yang**[1], **Yanlong Zhang**[1], **Yu Dong**[1], **Junhui Bi**[2], **Xiwen Liu**[3]

1. *College of Earth Sciences, Jilin University, Changchun 130061, China*
2. *Tianjin Center, China Geological Survey, Tianjin 300170, China*
3. *Jilin Provincial Water Resources and Hydropower Consultative Company, Changchun 130021, China*

Zheng Ji: https://orcid.org/0000-0003-4577-6577; Wenchun Ge: https://orcid.org/0000-0001-9254-757X

ABSTRACT: We present detailed geochronological, geochemical, and zircon Hf isotopic data for Late Paleozoic granitic rocks from Handagai and Zhonghe plutons in the Xing'an Block, NE China, aiming to provide constraints on their origin and tectonic implications. New zircon U-Pb ages indicate they were formed in the Late Devonian (ca. 379 Ma) immediately after a striking 50 Ma magmatic lull (ca. 430−380 Ma) in the Xing'an Block. Petrological and geochemical features suggest that the Handagai monzogranites and Zhonghe alkali-feldspar granites are I- and A-type granites, respectively, although both of them have high-K calc-alkaline features and positive zircon $\varepsilon_{Hf}(t)$ values (+3.47 to +10.77). We infer that the Handagai monzogranites were produced by partial melting of juvenile basaltic crustal materials under a pressure of <8−10 kbar, whereas the Zhonghe alkali-feldspar granites were generated by partial melting of juvenile felsic crustal materials at shallower depths ($P \leqslant 4$ kbar). Our results, together with published regional data, indicate their generation involves a subduction-related extensional setting. Slab break-off of the Hegenshan-Heihe oceanic plate may account for the subduction-related extensional setting, as well as the transformation of arc magmatism from the Early−Middle Devonian lull to the Late Devonian−Early Carboniferous flare-up in the Xing'an Block.

KEY WORDS: Late Devonian, granitoids, geochemistry, slab break-off, Hegenshan-Heihe Ocean, Xing'an Block.

0 INTRODUCTION

The Central Asian Orogenic Belt (CAOB) is sandwiched between the Siberian and Baltica cratons to the north and the Tarim and North China cratons to the south (Şengör et al., 1993). It stretches from the Caspian Sea to the Western Pacific Ocean for over 6 000 km, making the CAOB one of the largest orogenic systems on Earth (Windley et al., 2007). Unlike the typical collisional orogens, the CAOB formed by prolonged patchwork of island arcs, ophiolites, accretionary prisms, seamounts, oceanic plateaux, accretionary wedges, and microcontinents within the Paleo-Asian Ocean (PAO) during the Late Proterozoic to Mesozoic, and it therefore is regarded as a classical accretionary orogenic belt that marked the processes of the oceanic subduction and continental growth (Xiao et al., 2019; Xiao and Santosh, 2014).

Eastern part of CAOB is mainly occupied by northeastern (NE) China (Fig. 1a), which is characterized by the accretion and convergence of three blocks [i.e., the Erguna Block (EB), Xing'an Block (XB), and Songliao Block (SB)] related to subduction of the PAO during the Paleozoic (Wu et al., 2011). Previously, a number of studies have been carried out to reconstruct the locations of the suture zone and timing of the collision among these blocks (Yang et al., 2019; Ji et al., 2018; Liu et al., 2017). However, Late Paleozoic tectonic evolution of the XB remains debated, and lots of crucial problems have not been adequately solved, particularly the relationship between evolution of arc magmatism and subduction process of Hegenshan-Heihe Ocean (a northern branch of the PAO between the XB and SB). Although controversies still exist, growing evidence suggests that the XB was an active margin with extensive Ordovician−Carboniferous arc magmatism in response to the westward subduction of the Hegenshan-Heihe Ocean (Liu B et al., 2021; Gou et al., 2019; Feng et al., 2018; Liu Y J et al., 2017). Notably, two high-volume flare-ups of arc magmatism (i.e., the Early Ordovician−Late Silurian and Late Devonian−Early Carboniferous) were punctuated by a low-volume magmatic lull (i.e., Early−Middle Devonian) in the XB. However,

the driving mechanisms for the transformation of arc magmatism from the Early−Middle Devonian lull to the Late Devonian−Early Carboniferous flare-up remain uncertain and enigmatic. This is because that compared with the well-studied Early Carboniferous igneous rocks in the XB, there have been few studies of the Late Devonian igneous rocks that recorded the early process of Late Paleozoic magmatic flare-up. Although sparsely exposed, the Late Devonian igneous rocks could provide a good opportunity to understand the significant transformation of arc magmatism in the XB.

Here, we present new geochronological, whole-rock geochemical, and zircon Hf isotopic data for the Late Devonian granitoids in the XB. These new data, combined with the re-

sults of previous research, allow us to discuss the petrogenesis and tectonic environment of these granitoids and to provide new insights into Late Paleozoic deep geodynamic processes related to the subduction of the Hegenshan-Heihe Ocean.

1 GEOLOGICAL BACKGROUND

Western part of NE China, located in the eastern segment of the CAOB, evolved from amalgamation of the EB, XB, and SB as a result of the Paleozoic subduction and accretion of the PAO (Wu et al., 2011). These microcontinental blocks are separated by the Xinlin-Xiguitu and Hegenshan-Heihe suture zones, respectively.

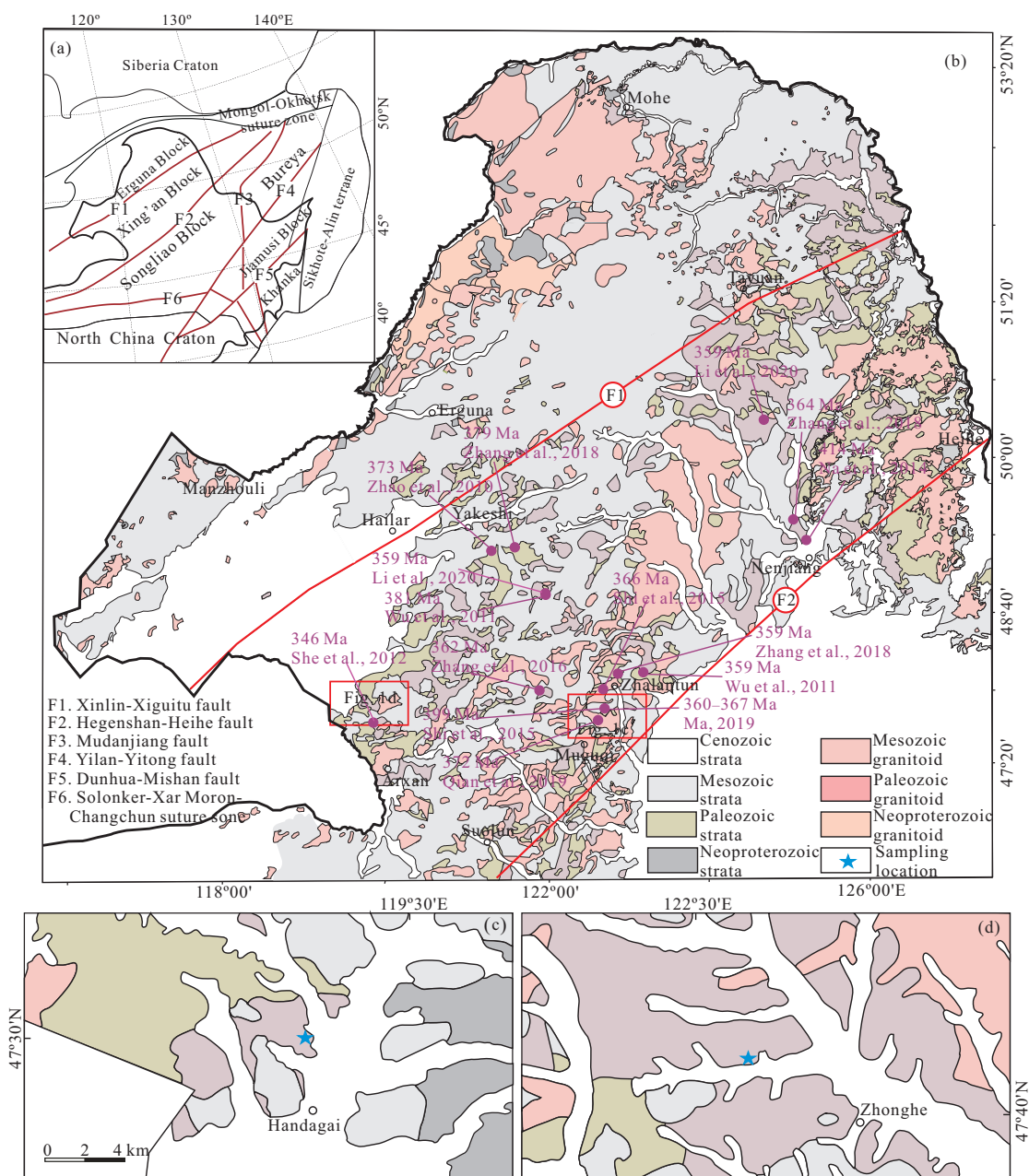The main body of the EB and XB consists mainly of Paleo-

Figure 1. (a) Tectonic subdivision of NE China and adjacent areas (modified from Wu et al., 2011). (b) Geological map of the XB-EB, showing the distribution of Devonian igneous rocks (modified after Li et al., 2017). Age data are from Li et al. (2020), Ma (2019), Qian et al. (2019), Zhang Y et al. (2018), Zhang Y J et al. (2016), Shi et al. (2015), Na et al. (2014), She et al. (2012), Wu et al. (2011), and Zhao et al. (2010). Geological map and sampling locations of (c) the Handagai and (d) Zhonghe area.

zoic granitoids and sedimentary strata covered/cut by voluminous Mesozoic volcanic rocks and granitoids (Fig. 1b). The EB is characterized by the occurrence of the Neoarchean−Proterozoic gneissic granitoids (ca. 2 600−700 Ma) and Neoproterozoic metamorphic supracrustal rocks (e.g., Xinhuadukou, Ergunahe, and Jiageda groups), which were considered as the Precambrian metamorphic basement. In contrast, no Precambrian rocks have been identified in the XB (Wu et al., 2011), although a few detrital zircons from the metasedimentary rocks in the Zalantun and Duobaoshan areas have ages varying from 2 952 to 566 Ma (Zhou et al., 2018). Thus, some scholars proposed that there was likely no Precambrian basement beneath the XB. Research on the Early Paleozoic high-pressure metamorphic rocks and post-orogenic granitoids along the Xinlin-Xiguitu suture zone reveals that the amalgamation of the EB and XB occurred at ca. 500 Ma (Zhou et al., 2015; Ge et al., 2005). Subsequently, a Late/Mddile Ordovician−Silurian arc-back-arc system developed in the integrated XB-EB in response to subduction of the Hegenshan-Heihe Ocean (Liu et al., 2021; Feng et al., 2018).

The SB is bounded by the XB in the northwest along the Hegenshan-Heihe suture zone and mainly covered by the Songliao Basin. The Songliao Basin is filled with thick Late Mesozoic−Cenozoic terrestrial strata. Its basement consists of deformed and metamorphosed Paleozoic−Mesozoic granitoids and Paleozoic volcanic-sedimentary strata (Wu et al., 2001). Recently, some Precambrian rocks were reported in the periphery of the Songliao Basin, including the Neoarchean trondhjemites (ca. 2.6 Ga) and Paleoproterozoic A-type granite (ca. 1.8 Ga) in the Longjiang area (Qian et al., 2018; Zhang et al., 2018), Paleoproterozoic deformed intrusive rocks (ca. 1.8 Ga) in the Gongzhuling area (Pei et al., 2007), and Neoproterozoic granitoids (ca. 929−841 Ma) in the Yichun area (Luan et al., 2019).

This study focuses on two granitic intrusions (i.e., Handagai and Zhonghe plutons) in the XB. The Handagai pluton, located near the Handagai Town, intrudes the Middle−Upper Ordovician Luohe Formation and is overlain by the Mesozoic−Cenozoic strata (Fig. 1c). The pluton is dominated by monzogranites that exhibit massive structures and contain plagioclase (30%−35%), alkali feldspar (30%−35%), quartz (25%−30%),

hornblende (5%−10%), and minor accessory minerals (Fig. 2a). The Zhonghe pluton, located near the Zhonghe Town, intrudes the previously defined Neoproterozoic Xinhuadukou Group and is overlain by the Lower Permian Dashizhai Formation and the Mesozoic−Cenozoic strata (Fig. 1b). The pluton is dominated by alkali feldspar granites with weakly gneissic structures. These alkali feldspar granites consist of alkali feldspar (45%−50%), quartz (40%−45%), plagioclase (5%−10%), and minor accessory minerals and hornblende (<3%) (Fig. 2b).

2 ANALYTICAL RESULTS

Analytical methods used during this study were presented in Appendix A.

2.1 Zircon U-Pb Ages

The zircons from the Handagai and Zhonghe plutons occur as euhedral crystals, and exhibit oscillatory zoning in CL images (Fig. 3). Their U and Th contents and Th/U ratios vary from 126 ppm to 3 890 ppm, 92 ppm to 2 440 ppm, and 0.09 to 1.34 (Table S1), respectively, indicative of a magmatic origin.

Sample 14GW488, a monzogranite, was collected from the Handagai pluton (location: 47°29′39.5″N, 119°25′48.2″E). Eighteen zircons were analyzed for the sample. Excluding 5 discordant analyses, the remaining 13 concordant analyses produce $^{206}Pb/^{238}U$ ages of 461−370 Ma, with two groups: 458 ± 3 Ma (mean squared weighted deviation (MSWD) = 0.78; $n = 4$) and 379 ± 4 Ma (MSWD = 4.20; $n = 9$) (Fig. 3a). The younger age of 379 Ma is interpreted as the crystallization age of the monzogranite.

Sample 13GW243, an alkali feldspar granite, was collected from the Zhonghe pluton (location: 47°41′21.2″N, 122°31′26.8″E). Twenty-five zircons were analyzed for the sample. Their $^{206}Pb/^{238}U$ ages range from 380 to 376 Ma, and form a group with a weighted mean $^{206}Pb/^{238}U$ age of 379 ± 1 Ma (MSWD = 0.39; $n = 25$) (Fig. 3b), representing the crystallization age of the rock.

2.2 Major and Trace Elements
2.2.1 Handagai pluton

The Late Devonian monzogranite samples from the Handagai pluton have SiO_2 contents of 67.15 wt.%−69.84 wt.%,
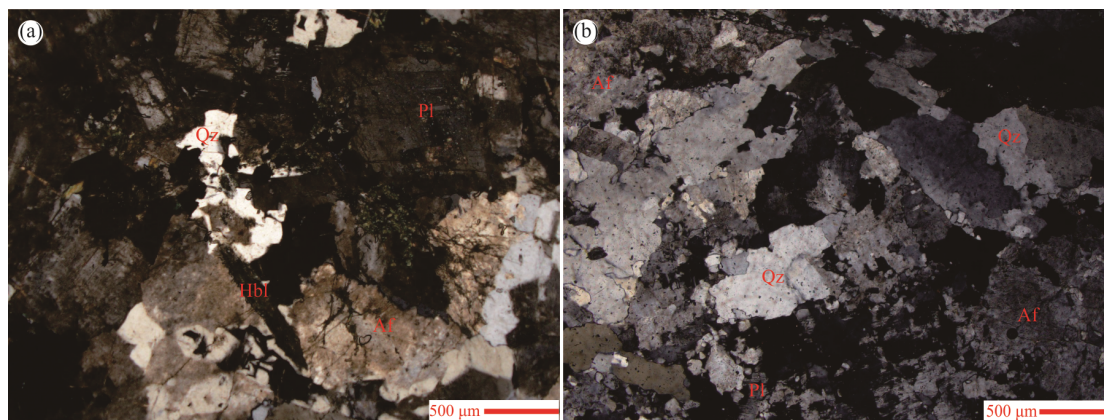

Figure 2. Microphotographs of the Late Devonian granitoids from the XB. (a) Handagai monzogranite (sample 14GW491); (b) Zhonghe alkali feldspar granite (13GW343). Af. Alkali feldspar; Hbl. hornblende; Pl. plagioclase; Qz. quartz.
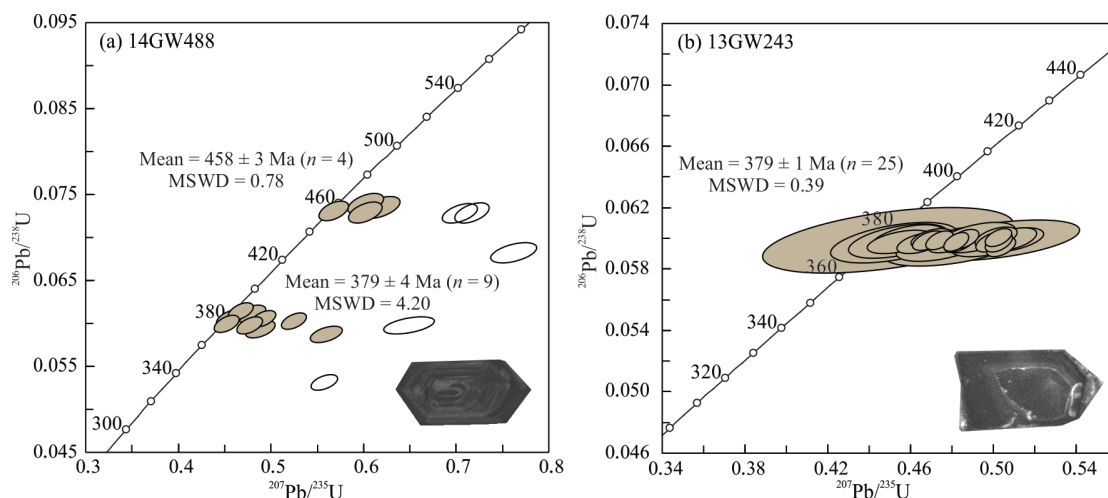
Figure 3. Zircon U-Pb concordia diagrams for the Late Devonian granitoids from the XB, with representative CL images of analyzed zircon grains.
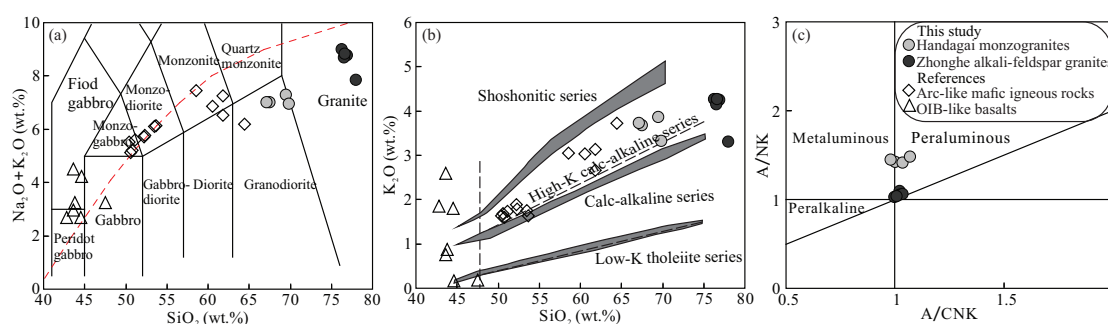

Figure 4. Plots of (a) $Na_2O + K_2O$ vs. SiO_2 (after Irvine and Baragar, 1971), (b) K_2O vs. SiO_2 (after Peccerillo and Taylor, 1976), and (c) A/NK vs. A/CNK (after Maniar and Piccoli, 1989) for the Late Devonian granitoids from the XB. Data for the Late Devonian arc-like mafic igneous rocks in the Zhalantun area of the XB are from Qian et al. (2019) and Zhang et al. (2016), whereas data for the Late Devonian OIB-like basalts in the Zhalantun area of the XB are from Zhang et al. (2016).

K_2O of 3.32 wt.%−3.86 wt.%, Na_2O of 3.27 wt.%−3.62 wt.%, Al_2O_3 of 13.40 wt.% −14.15 wt.% , CaO of 1.96 wt.% −2.46 wt.%, MgO of 0.24 wt.%−0.86 wt.%, and TFe_2O_3 of 2.93 wt.%− 3.52 wt.% (Table S2). They belong to high-K calc-alkaline series and metaluminous to weakly peraluminous rocks (A/CNK = 0.98−1.08) (Fig. 4). Their chondrite-normalized REE patterns are marked by moderate enrichment of light rare earth elements (LREEs) $[(La/Yb)_N = 5.15−7.66]$ and negative Eu anomalies (Eu/Eu* = 0.44−0.55) (Fig. 5a). These rocks are enriched in Rb, Th, and U and depleted in Ba, P, and Ti (Fig. 5b).

2.2.2 Zhonghe pluton

The Late Devonian alkali-feldspar granite samples from the Zhonghe pluton have high SiO_2 (76.25 wt.%−77.97 wt.%), K_2O (3.30 wt.%−4.27 wt.%), and $Na_2O + K_2O$ (7.84 wt.%− 8.99 wt.%) contents, belonging to high-K calc-alkaline series (Fig. 4). They show low Al_2O_3 (12.07 wt.%−12.69 wt.%), CaO (0.16 wt.% −0.43 wt.%), MgO (0.05 wt.% −0.08 wt.%), and TFe_2O_3 (0.82 wt.%−1.31 wt.%) contents, with corresponding A/CNK ratios of 1.00−1.03 and $Mg^\#$ values of 8−16, indicating that they are weakly peraluminous rocks. These rocks are negligible enrichment in LREEs relative to heavy rare earth elements (HREEs) $[(La/Yb)_N = 1.20−2.85]$, with strong negative Eu anomalies (Eu/Eu* = 0.03−0.07) (Fig. 5a). In the primitive mantle (PM)-normalized spider diagram, they display distinct

enrichment of large ion lithophile elements (LILEs; e. g., Rb, Th, U, and K) and depletion of Ba, P, Eu, and Ti (Fig. 5b).

2.3 Zircon Hf Isotopic Compositions

Magmatic zircons from monzogranite sample 14GW488 have initial $^{176}Hf/^{177}Hf$ ratios of 0.282 778 to 0.282 850, $\varepsilon_{Hf}(t)$ values of +8.34 to +10.77, and T_{DM2} ages of 845 to 722 Ma (Table S3). The initial $^{176}Hf/^{177}Hf$ ratios, $\varepsilon_{Hf}(t)$ values, and T_{DM2} ages for inherited zircon with age of 458 Ma are from 0.282 744 to 0.282 787, +8.74 to +10.29, and 879 to 781 Ma, respectively. Magmatic zircons from alkali feldspar granite sample 13GW243 have initial $^{176}Hf/^{177}Hf$ ratios of 0.282 656 to 0.282 831, $\varepsilon_{Hf}(t)$ values of +3.47 to +9.52, and two-stage model (T_{DM2}) ages of 1 155 to 769 Ma (Fig. 6).

3 DISCUSSION

3.1 Devonian Magmatism in the Xing'an Block

The Handagai and Zhonghe plutons were previously considered to be Triassic and Paleoproterozoic in age, based on lithostratigraphic relationships and regional comparisons (IMB-GMR, 1991). However, these ages had not been constrained by isotopic geochronological data. Here, we carried out zircon U-Pb dating on the granitoids from the Handagai and Zhonghe plutons to precisely determine their formation ages.

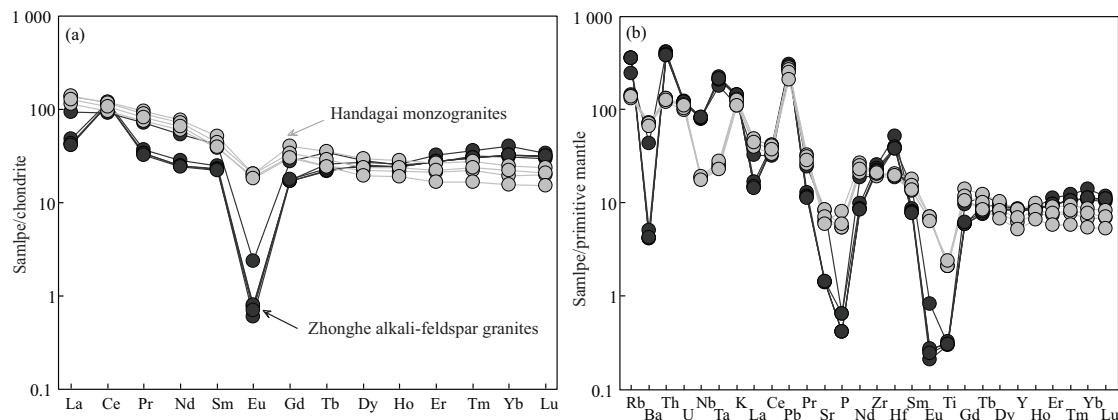Almost all zircons from the studied granitoid samples dis-

Figure 5. (a) Chondrite-normalized REE and (b) PM-normalized multi-element variation diagrams for the Late Devonian granitoids from the XB. The values of chondrite and PM values are from Sun and McDonough (1989).
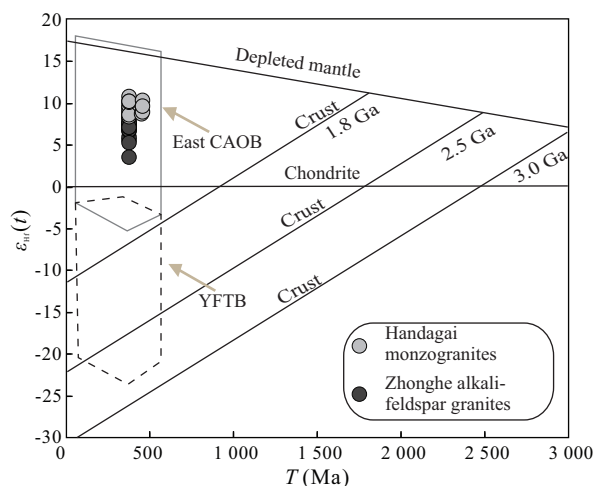

Figure 6. Diagram showing variations in $\varepsilon_{Hf}(t)$ vs. T (Ma) values for the Late Devonian granitoids from the XB (modified from Yang et al., 2006a). YFTB. Yanshan fold and thrust belt.

Figure 7. Probability plots of the zircon U-Pb ages for the Ordovician−Carboniferous igneous rocks in XB-EB. Age data are from Liu et al. (2021), Li et al. (2020), Ma (2019), Zhang et al. (2018), She et al. (2012), Wu et al. (2011), and references therein.

play oscillatory zoning, and have high Th/U ratios, indicating a magmatic origin. Accordingly, the zircon U-Pb ages for granitoids from the Handagai and Zhonghe plutons represent their formation ages. The Handagai monzogranites and Zhonghe alkali-feldspar granites were formed contemporaneously, with identical age of 379 Ma, i.e., Late Devonian. In addition to our study, some Late Devonian igneous rocks have also been identified in other areas of the XB, mainly including (1) the 373−359 Ma mylonitized monzonites, syenogranites, alkali-feldspar granites, andesites, and basaltic andesites in the Zhalantun-Nenjiang-Huolongmen area of the eastern XB (Qian et al., 2019; Zhang Y et al., 2018; Zhang Y J et al., 2016; Shi et al., 2015; Wu et al., 2011), (2) the 381−359 Ma granites, quartz diorites, and diorites in the Handagai-Boketu-Nuoming area of the central XB (Li et al., 2020; She et al., 2012; Wu et al., 2011), (3) the 379−373 Ma basalts and rhyolites in the Yakeshi area of the western XB (Zhang et al., 2018; Zhao et al., 2010). Given the above, we proposed that an important Late Devonian magmatic event occurred in XB with an approximately NE orientation. In addition, to better understand geochronological framework of the Paleozoic magmatism in the XB-EB, we compiled the available ages of the Ordovician−Carboniferous igneous
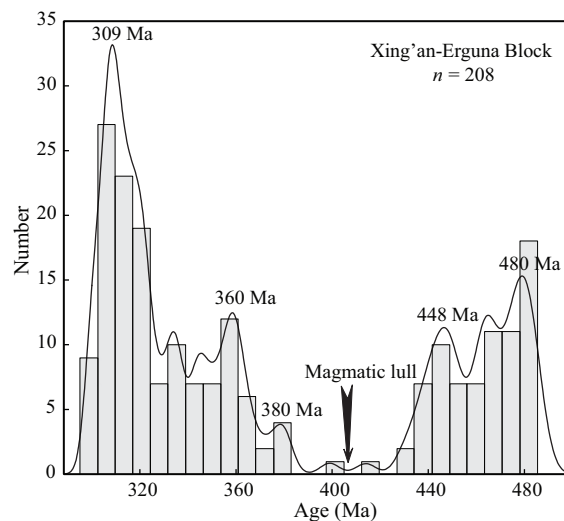
rocks. Our data compilation shows two stages of magmatic flare-ups in the XB-EB, i.e., in the Ordovician−Late Silurian at 458−430 Ma and in Late Devonian−Carboniferous at 380−298 Ma, with a striking magmatic lull between them (Fig. 7).

3.2   Petrogenesis of the Late Devonian Granitoids
3.2.1   Petrogenetic type

The possibility that the Late Devonian Handagai and Zhonghe plutons belong to M-type granites can be ruled out based on their low Cr (0.91 ppm−24.40 ppm) and Ni (1.46 ppm−7.86 ppm) contents and Mg# values (7−33). These plutons are metaluminous to weakly peraluminous (A/CNK = 0.98−1.08), and lack peraluminous minerals in contrast to S-type granites (Clemens, 2003). Low ($Na_2O + K_2O$)/CaO (2.85−3.71) and 10 000 × Ga/Al (2.16−2.32) values and Zr + Nb + Ce + Y contents (315 ppm−350 ppm) of the Handagai monzogranites, along with the occurrence of hornblende, suggest that the monzogranites belong to I-type granites. Compared with the Handagai monzogranites, the Zhonghe alkali-feldspar granites have higher ($Na_2O + K_2O$)/CaO (18.36−55.21) and 10 000 × Ga/Al

(3.55−4.09) values and Zr + Nb + Ce + Y contents (372 ppm−449 ppm), showing typical geochemical characteristics of A-type granites. Moreover, high SiO_2 contents (76.25 wt.%−77.97 wt.%) and zircon saturation temperatures (T_{Zr} = 818−836 °C) and remarkably negative Eu anomalies of the Zhonghe alkali-feldspar granites are also simialr to those of A-type granites. Additionally, in the discrimination diagrams of Eby (1990) and Whalen et al. (1987), rocks from the Zhonghe pluton plot in the A-type field (Fig. 8). In summary, the Handagai monzo-granites can be classified as I-type granites, and the Zhonghe alkali-feldspar granites belong to A-type granites.

3.2.2 Origin of I-type granites

The Handagai I-type granites have high Zr/Hf (36.04−39.28) and Nb/Ta (11.84−13.20) ratios and low Rb/Sr ratios (0.47−0.69) and differentiation index values (DI, 78−82), indicating the magmas that formed the rocks underwent limited fractionation crystallization. This is also manifested in their distribution into the unfractionated field in the discrimination diagrams (Fig. 8). Thus, geochemical compositions of the Handagai I-type granites can roughly assess the source characteristics. The Handagai I-type granites show high SiO_2 contents (67.15 wt.%−69.82 wt.%), low Cr (8.38 ppm−24.40 ppm) and Ni (5.26 ppm−7.86 ppm) contents and $Mg^{\#}$ values (12−33), and narrow range of $\varepsilon_{Hf}(t)$ (+8.34 to +10.77), indicating they were generated by the partial melting of crustal materials, without involvement of mantle-derived mafic magmas. The absence of mafic enclaves and mingling textures also supports this inference. The Handagai I-type granites are metaluminous-weakly peraluminous, high-K calc-alkaline rocks, similar in composition to felsic melts genereted by melting of moderate-ly hydrous medium/high-K basaltic rocks (Sisson et al., 2005). Moreover, all the samples plot in medium/high-K basaltic rock field in K_2O-SiO_2, Na_2O-SiO_2 and K_2O-Na_2O-CaO diagrams (Figs. 9a, 9b, 9c). In combination with positive $\varepsilon_{Hf}(t)$ values (+8.34 to +10.77) and juvenile T_{DM2} ages (845−722 Ma), we proposed that primary magmas of the Handagai I-type granites were generated by partial melting of a dominantly juvenile, medium/high-K, basaltic crustal materials. Additionally, the Handagai I-type granites are depleted in Sr (125 ppm−176 ppm), and have moderately negative Eu anomalies (0.44 ppm−0.55 ppm), suggesting residual plagioclase in the source. These

rocks also contain moderate Yb (2.65 ppm−4.23 ppm) and Y (23.60 ppm−37.80 ppm) contents, and have concave-upward shaped REE patterns between the middle and heavy REEs, indicating the breakdown of garnet and the presence of residual hornblende during partial melting of the basaltic crust (Rollinson, 1993). These characteristics argue for magma formation under a pressure of <8−10 kbar (Zhang et al., 2010). Overall, it is concluded that the Handagai I-type granites were generated by partial melting of juvenile, medium/high-K, basaltic crustal materials under a pressure of <8−10 kbar.

3.2.3 Origin of A-type granites

Several models have been proposed to explain origin of the A-type granites, including: (1) fractional crystallization of mafic magmas (Turner et al., 1992); (2) mixing between felsic and mafic magmas (Yang et al., 2006b; Kemp et al., 2005); and (3) partial melting of crustal materials, such as granulitic metasedimentary rocks (Huang et al., 2011), lower-crustal granulite residues from which hydrous felsic melts had been previously extracted (Collins et al., 1982), calc-alkaline granitoids (Frost and Frost, 2011; Patiño Douce, 1997).

Given the appearance of contemporaneous mantle-derived mafic igneous rocks in the Zhalantun area (Qian et al., 2019; Zhang et al., 2016), it is easy to consider a mafic magma progenitor or contributor for the origin of the Zhonghe A-type granites. However, such petrogenetic models are infeasible. First of all, the predominance of the Late Devonian granitoids in volume over contemporaneous mafic igneous rocks and the obvious compositional gap between the two are inconsistent with a magma differentiation model that is characterized by plenty of contemporaneous mafic igneous rocks and a continuous compositional trend. Secondly, the Zhonghe A-type granites have high SiO_2 contents (76.25 wt.%−77.97 wt.%), low Cr (0.91 ppm−2.57 ppm) and Ni (1.46 ppm−1.61 ppm) contents and $Mg^{\#}$ values (7−16), and homogeneous Hf isotopic compositions, indicating a negligible contribution from mafic magmas. Finally, there is no petrological evidence (e.g., complex compositional zoning in minerals and mafic microgranular enclaves in rocks) for mixing between felsic and mafic magmas. Thus, the first two petrogenesis models are unavailable for the Zhonghe A-type granites.
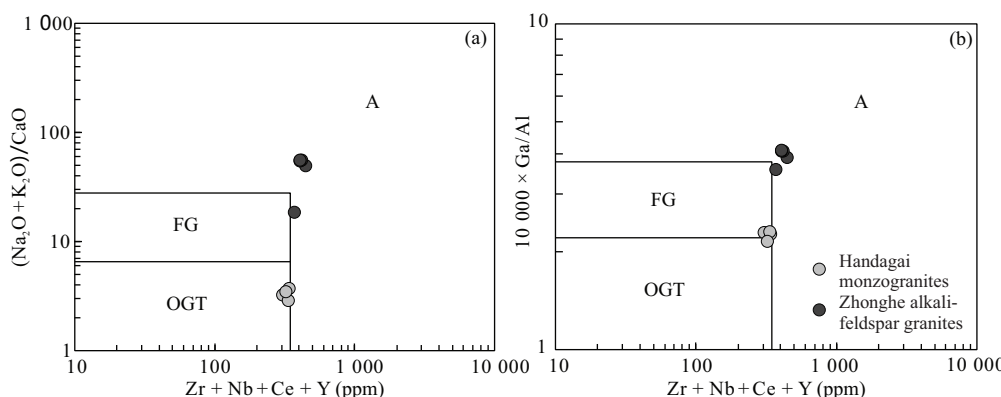

Figure 8. Plots of (a) (Na_2O + K_2O)/CaO vs. Zr + Nb + Ce + Y (after Eby, 1990) and (b) 10 000 × Ga/Al vs. Zr + Nb + Ce + Y (after Whalen et al., 1987) for the Late Devonian granitoids from the XB. FG. highly fractionated I-type granites; OGT. unfractionated I-, S-, and M-type granites; A. A-type granites.
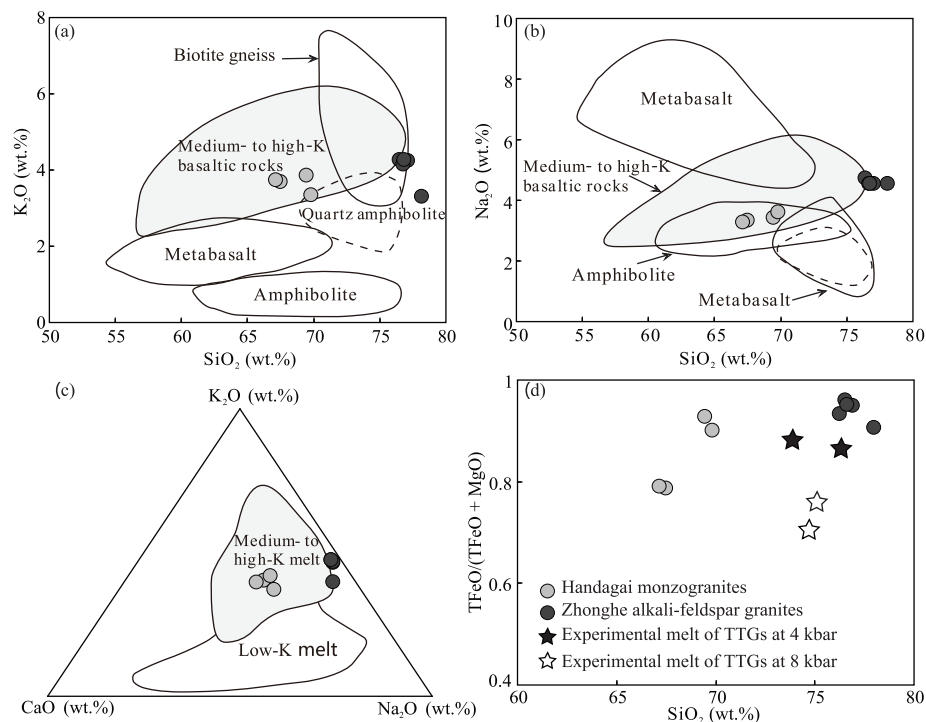
Figure 9. (a) K_2O-SiO_2, (b) Na_2O-SiO_2 (Zhang et al., 2017), (c) K_2O-Na_2O-CaO (Guo et al., 2012), and (d) FeOT/(FeOT + MgO)-SiO_2 (Bi et al., 2016) diagrams for the Late Devonian granitoids from the XB.

Magmas originated from the refractory granulitic residues are depleted in TiO_2 relative to MgO and alkalis relative to alumina (Creaser et al., 1991). However, the Zhonghe A-type granites have high $(Na_2O + K_2O)/Al_2O_3$ (18−55) and TiO_2/MgO (0.87−1.33) ratios, precluding a granulitic residual origin. In addition, the Zhonghe A-type granites are weakly peraluminous, which is in contrast to the metasedimentary source, as this produces melts with a strongly peraluminous signature. Experimental research has shown that high-temperature melting of calc-alkaline granitoids can generate A-type granitic melts (Bogaerts et al., 2006; Patiño Douce, 1997; Skjerlie and Johnston, 1993). Notably, low-pressure conditions ($P \leqslant 4$ kbar) yiled metaluminous to weakly peraluminous A-type granitic melts, whereas high-pressure conditions ($P \geqslant 8$ kbar) generate strongly peraluminous A-type granitic melts (Frost and Frost, 2011). Considering their weakly peraluminous signatures and high T_{Zr} values, SiO_2 contents, and TFeO/(TFeO + MgO) ratios (Fig. 9d), we suggest that the Zhonghe A-type granites were generated by the high-temperature partial melting of calc-alkaline granitic rocks under low-pressure conditions. The low-pressure conditions are also favored by the low $(La/Yb)_N$ (1.20−2.85) and Sr/Y (0.78−4.39) ratios, high Yb (5.27 ppm−6.93 ppm) and Y contents (37 ppm−39 ppm), and distinctly negative Ba, Sr and Eu anomalies. Collectively, given the positive $\varepsilon_{Hf}(t)$ values (+3.47 to +9.52) and juvenile T_{DM2} ages (1 155−769 Ma), we propose that the Zhonghe A-type granites were derived by high-temperature partial melting of juvenile felsic crustal materials under a pressure of ≤4 kbar.

3.3   Implications for the Late Devonian Slab Break-off during Subduction of the Hegenshan-Heihe Ocean

High-K calc-alkaline I- and A-type granites are commonly considered to occur in a variety of extensional regimes, including post-collision extensional settings and subduction-related extensional settings (Badr et al., 2018; Yin et al., 2017; Zhao J L et al., 2016; Wu et al., 2012; Zhao X F et al., 2008; Li et al., 2007; Eby, 1990). The Late Devonian Handagai and Zhonghe plutons have geochemical affinities with high-K calc-alkaline I- and A-type granites, respectively, suggesting a predominantly extensional environment. Nonetheless, the question remains as to what geodynamic mechanism can induce the Late Devonian regional extension in the XB.

Some researchers have proposed that the PAO between the XB and SB closed before the Middle Devonian along the Airgin Sum-Xilinhot-Heihe suture zone (Xu et al., 2015, 2013). That means the whole period of the Late Devonian−Early Carboniferous magmatism formed in a post-collision extensional setting. However, the model is inconsistent with the following lines of geological evidence: (1) the Upper Devonian−Lower Carboniferous strata in the XB (e.g., Daminshan, Hongshuiquan, and Moergenhe formations consisting of carbonate rocks, clastic rocks, chert, and volcanic rocks) were formed in the marine sedimentary environment (Zhao et al., 2012; IMB-GMR, 1991), indicating the ocean basin was still in existence during the Late Devonian−Early Carboniferous; (2) there is a lack of the Devonian molasse-like sediments in the XB, indicating terminal collision between the XB and SB did not occur during the Devonian; and (3) the Late Devonian mafic igneous rocks in the XB (i.e., ca. 373 Ma Yakeshi basalts, 381−359 Ma Boketu quartz diorites and diorites, and 373−362 Ma Zhalantun andesites and basaltic andesites) are characterized by enrichment in LILEs and depletion in HFSEs, with distinct Nb, Ta, and Ti troughs (Qian et al., 2019; Zhang et al., 2016; Wu et al., 2011; Zhao et al., 2010), similar to geochemical features of

active continental margin volcanics, indicating the Late Devonian westward subduction of the Hegenshan-Heihe Ocean beneath the XB. The above lines of evidence undoubtedly suggest that XB was in a subduction-related extensional setting instead of a post-collision extensional setting during the Late Devonian.

Two principal mechanisms have been proposed to account for subduction-related extensional settings: (a) slab roll-back (Ji et al., 2019; Niu, 2018; Yin et al., 2017; Zhao et al., 2016; Liu et al., 2014) and (b) slab break-off (Bi et al., 2016; Zhu et al., 2016; Li and Li, 2007; Li et al., 2007). Although both mechanisms could induce asthenospheric upwelling and lithospheric extension in a subduction setting, magmatism resulted from slab roll-back and break-off would display different spatial and temporal distribution. Under gravity and with the continued subduction, the dip angle of subducting slab would increase gradually as the slab rotates vertically, leading to slab roll-back (Niu, 2018). As a result, the arc magmatism in the overlying plate would migrate toward the trench (Ji et al., 2019; Liu et al., 2014). However, Late Devonian magmatic rocks in XB parallel to the Hegenshan-Heihe suture zone without a trenchward-younging trend. Furthermore, slab roll-back would produce A-type granites located near the back-arc position, contrasting with the case in the XB. Accordingly, we consider a slab roll-back model fails to explain Late Devonian subduction-related extensional setting in the XB.

Break-off of subducting lithospheric slabs is a process well recognized in many subduction systems worldwide and documented by geophysical observations (Rosenbaum et al., 2008; Gerya et al., 2004). Slab break-off is commonly considered to be associated with the early stages of continental collision owing to a decrease in the subduction rate damped by arrival of buoyant continental lithosphere at subduction region (Huw Davies and von Blanckenburg, 1995). Nevertheless, slab break-off may also be triggered by a decrease in subduction rate in other geodynamic settings (Bi et al., 2016; Zhu et al.,

2016; Li et al., 2007; Li and Li, 2007; Gerya et al., 2004). Li and Li (2007) used a break-off of the flat-subducting oceanic slab model to explain the Jurassic−Cretaceous magmatic flare-up and lithospheric extension in southeastern China. Here, we adopt this model to decipher the geodynamic mechanism of the Late Devonian subduction-related extension in the XB. The Late Devonian−Early Carboniferous (ca. 380−330 Ma) subduction-induced magmatic flare-up appeared about 50 Ma later after the termination of the Ordovician−Late Silurian (ca. 458−430 Ma) flare-up, and such a long quiescent period of arc magmatism is consistent with low-angle/flat-slab subduction of the Hegenshan-Heihe oceanic plate (Li and Li, 2007; Gutscher et al., 2000; Fig. 10a). After the low-angle/flat-slab subduction of the Hegenshan-Heihe oceanic plate reached its maxima due to its strong coupling with the overriding continental lithosphere, the low-velocity subducting slab started to break off. A direct response to the slab break-off is the upwelling of fresh, hot asthenospheric mantle materials that can initiate melting of the metasomatized lithospheric mantle, asthenospheric mantle, and continental crust and magmatism of different chemistry from arc type to ocean island basalt (OIB) type (Prelević et al., 2015). The appearance of the Late Devonian A-type granites, arc-type basaltic andesites and andesites, and OIB-type basalts in the Zhalantun area of the XB indicates the beginning of slab break-off, which resulted in a high-temperature and extensional subduction setting in the XB during the Late Devonian (Fig. 10b).

In summary, we conclude that slab break-off of the Hegenshan-Heihe oceanic plate possibly occurred in the Late Devonian, and that it led to a transformation of arc magmatism from the Early−Middle Devonian lull to the Late Devonian−Early Carboniferous flare-up in the XB.

4   CONCLUSIONS

(1) Zircon U-Pb dating results indicate that the Handagai monzogranites and Zhonghe alkali-feldspar granites in the XB formed contemporaneously in the Late Devonian (ca. 379 Ma).
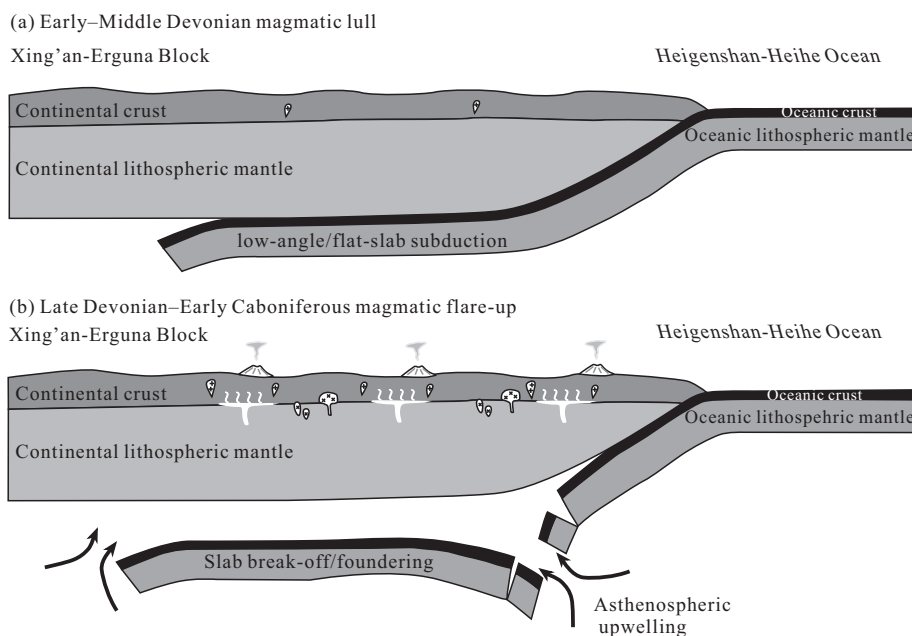

Figure 10. Tectonic model illustrating the Late Paleozoic subduction system in the XB-EB (modified from Li and Li, 2007).

(2) The Handagai monzogranites are I-type granites, and formed by partial melting of juvenile, medium/high-K, basaltic crustal materials under a pressure of <8–10 kbar. The Zhonghe alkali-feldspar granites are A-type granites, and formed by high-temperature partial melting of juvenile felsic crustal materials at relatively shallow depths.

(3) A slab break-off of the Hegenshan-Heihe Ocean model is proposed for late Paleozoic tectonic evolution of the XB.

ACKNOWLEDGMENTS

Electronic Supplementary Materials: Supplementary materials (Tables S1–S3, Appendix A) are available in the online version of this article at https://doi.org/10.1007/s12583-021-1497-9.

REFERENCES CITED

Badr, A., Davoudian, A. R., Shabanian, N., et al., 2018. A- and I-Type Metagranites from the North Shahrekord Metamorphic Complex, Iran: Evidence for Early Paleozoic Post-Collisional Magmatism. *Lithos*, 300/301: 86–104. https://doi.org/10.1016/j.lithos.2017.12.008

Bi, J. H., Ge, W. C., Yang, H., et al., 2016. Geochronology and Geochemistry of Late Carboniferous–Middle Permian I- and A-Type Granites and Gabbro-Diorites in the Eastern Jiamusi Massif, NE China: Implications for Petrogenesis and Tectonic Setting. *Lithos*, 266/267: 213–232. https://doi.org/10.1016/j.lithos.2016.10.001

Bogaerts, M., Scaillet, B., Auwera, J. V., 2006. Phase Equilibria of the Lyngdal Granodiorite (Norway): Implications for the Origin of Metaluminous Ferroan Granitoids. *Journal of Petrology*, 47(12): 2405–2431. https://doi.org/10.1093/petrology/egl049

Clemens, J. D., 2003. S-Type Granitic Magmas—Petrogenetic Issues, Models and Evidence. *Earth-Science Reviews*, 61(1/2): 1–18. https://doi.org/10.1016/S0012-8252(02)00107-1

Collins, W. J., Beams, S. D., White, A. J. R., et al., 1982. Nature and Origin of A-Type Granites with Particular Reference to Southeastern Australia. *Contributions to Mineralogy and Petrology*, 80(2): 189–200. https://doi.org/10.1007/BF00374895

Creaser, R. A., Price, R. C., Wormald, R. J., 1991. A-Type Granites Revisited: Assessment of a Residual-Source Model. *Geology*, 19(2): 163. https://doi.org/10.1130/0091-7613(1991)0190163:atgrao>2.3.co;2

Eby, G. N., 1990. The A-Type Granitoids: a Review of Their Occurrence and Chemical Characteristics and Speculations on Their Petrogenesis. *Lithos*, 26(1/2): 115–134. https://doi.org/10.1016/0024-4937(90)90043-z

Feng, Z. Q., Liu, Y. J., Wu, P., et al., 2018. Silurian Magmatism on the Eastern Margin of the Erguna Block, NE China: Evolution of the Northern Great Xing'an Range. *Gondwana Research*, 61: 46–62. https://doi.org/10.1016/j.gr.2018.04.011

Frost, C. D., Frost, B. R., 2011. On Ferroan (A-Type) Granitoids: Their Compositional Variability and Modes of Origin. *Journal of Petrology*, 52(1): 39–53. https://doi.org/10.1093/petrology/egq070

Ge, W. C., Wu, F. Y., Zhou, C. Y., et al., 2005. Emplacement Age of the Tahe Granite and Its Constraints on the Tectonic Nature of the Ergun

Block in the Northern Part of the Da Hinggan Range. *Chinese Science Bulletin*, 18: 2097–2105 (in Chinese)

Gerya, T. V., Yuen, D. A., Maresch, W. V., 2004. Thermomechanical Modelling of Slab Detachment. *Earth and Planetary Science Letters*, 226(1/2): 101–116. https://doi.org/10.1016/j.epsl.2004.07.022

Gou, J., Sun, D. Y., Yang, D. G., et al., 2019. Late Palaeozoic Igneous Rocks of the Great Xing'an Range, NE China: The Tayuan Example. *International Geology Review*, 61(3): 314–340. https://doi.org/10.1080/00206814.2018.1425923

Guo, F., Fan, W. M., Li, C. W., et al., 2012. Multi-Stage Crust-Mantle Interaction in SE China: Temporal, Thermal and Compositional Constraints from the Mesozoic Felsic Volcanic Rocks in Eastern Guangdong-Fujian Provinces. *Lithos*, 150: 62–84. https://doi.org/10.1016/j.lithos.2011.12.009

Gutscher, M. A., Maury, R., Eissen, J. P., et al., 2000. Can Slab Melting be Caused by Flat Subduction?. *Geology*, 28(6): 535–538. https://doi.org/10.1130/0091-7613(2000)28535:csmbcb>2.0.co;2

Huang, H. Q., Li, X. H., Li, W. X., et al., 2011. Formation of High ^{18}O Fayalite-Bearing A-Type Granite by High-Temperature Melting of Granulitic Metasedimentary Rocks, Southern China. *Geology*, 39(10): 903–906. https://doi.org/10.1130/g32080.1

Huw Davies, J., von Blanckenburg, F., 1995. Slab Breakoff: A Model of Lithosphere Detachment and Its Test in the Magmatism and Deformation of Collisional Orogens. *Earth and Planetary Science Letters*, 129(1/2/3/4): 85–102. https://doi.org/10.1016/0012-821x(94)00237-s

IMBGMR (Inner Mongolian Bureau of Geology Mineral Resources), 1991. Regional Geology of Inner Mongolia. Geological Publishing House, Beijing. 1–725 (in Chinese with English Abstract)

Irvine, T. N., Baragar, W. R. A., 1971. A Guide to the Chemical Classification of the Common Volcanic Rocks. *Canadian Journal of Earth Sciences*, 8(5): 523–548. https://doi.org/10.1139/e71-055

Ji, Z., Ge, W. C., Yang, H., et al., 2018. Late Carboniferous–Early Permian High- and Low-Sr/Y Granitoids of the Xing'an Block, Northeastern China: Implications for the Late Paleozoic Tectonic Evolution of the Eastern Central Asian Orogenic Belt. *Lithos*, 322: 179–196. https://doi.org/10.1016/j.lithos.2018.10.014

Ji, Z., Meng, Q. A., Wan, C. B., et al., 2019. Geodynamic Evolution of Flat-Slab Subduction of Paleo-Pacific Plate: Constraints from Jurassic Adakitic Lavas in the Hailar Basin, NE China. *Tectonics*, 38(12): 4301–4319. https://doi.org/10.1029/2019tc005687

Kemp, A. I. S., Wormald, R. J., Whitehouse, M. J., et al., 2005. Hf Isotopes in Zircon Reveal Contrasting Sources and Crystallization Histories for Alkaline to Peralkaline Granites of Temora, Southeastern Australia. *Geology*, 33(10): 797–800. https://doi.org/10.1130/g21706.1

Li, X. H., Li, Z. X., Li, W. X., et al., 2007. U-Pb Zircon, Geochemical and Sr-Nd-Hf Isotopic Constraints on Age and Origin of Jurassic I- and A-Type Granites from Central Guangdong, SE China: A Major Igneous Event in Response to Foundering of a Subducted Flat-Slab?. *Lithos*, 96(1/2): 186–204. https://doi.org/10.1016/j.lithos.2006.09.018

Li, Y., Xu, W. L., Tang, J., et al., 2020. Late Paleozoic Igneous Rocks in the Xing'an Massif and Its Amalgamation with the Songnen Massif, NE China. *Journal of Asian Earth Sciences*, 197: 104407. https://doi.org/10.1016/j.jseaes.2020.104407

Li, Y., Xu, W. L., Wang, F., et al., 2017. Triassic Volcanism along the Eastern Margin of the Xing'an Massif, NE China: Constraints on the Spatial-Temporal Extent of the Mongol-Okhotsk Tectonic Regime. *Gondwana Research*, 48: 205–223. https://doi.org/10.1016/j.gr.

2017.05.002

Li, Z. X., Li, X. H., 2007. Formation of the 1 300-km-Wide Intracontinental Orogen and Postorogenic Magmatic Province in Mesozoic South China: A Flat-Slab Subduction Model. *Geology*, 35(2): 179−182. https://doi.org/10.1130/g23193a.1

Liu, B., Chen, J. F., Han, B. F., et al., 2021. Geochronological and Geochemical Evidence for a Late Ordovician to Silurian Arc-Back-Arc System in the Northern Great Xing'an Range, NE China. *Geoscience Frontiers*, 12(1): 131−145. https://doi.org/10.1016/j.gsf.2020.07.002

Liu, L., Xu, X. S., Xia, Y., 2014. Cretaceous Pacific Plate Movement beneath SE China: Evidence from Episodic Volcanism and Related Intrusions. *Tectonophysics*, 614: 170−184. https://doi.org/10.1016/j.tecto.2013.12.007

Liu, Y. J., Li, W. M., Feng, Z. Q., et al., 2017. A Review of the Paleozoic Tectonics in the Eastern Part of Central Asian Orogenic Belt. *Gondwana Research*, 43: 123−148. https://doi.org/10.1016/j.gr.2016.03.013

Luan, J. P., Yu, J. J., Yu, J. L., et al., 2019. Early Neoproterozoic Magmatism and the Associated Metamorphism in the Songnen Massif, NE China: Petrogenesis and Tectonic Implications. *Precambrian Research*, 328: 250−268. https://doi.org/10.1016/j.precamres.2019.04.004

Ma, Y. F., 2019. The Late Paleozoic Tectonic Evolution of the Central Great Xing'an Range, NE China: [Dissertation]. Jilin University, Changchun (in Chinese with English Abstract)

Maniar, P. D., Piccoli, P. M., 1989. Tectonic Discrimination of Granitoids. *Geological Society of America Bulletin*, 101(5): 635−643. https://doi.org/10.1130/0016-7606(1989)1010635:tdog>2.3.co;2

Na, F. C., Fu, J. Y., Wang, Y., et al., 2014. LA-ICP-MS Zircon U-Pb Age of the Chlorite-Muscovite Tectonic Schist in Hadayang, Morin Dawa Banner, Inner Mongolia, and Its Tectonic Significance. *Geological Bulletin of China*, 33(9): 1326−1332 (in Chinese with English Abstract)

Niu, Y. L., 2018. Geological Understanding of Plate Tectonics: Basic Concepts, Illustrations, Examples and New Perspectives. *Global Tectonics and Metallogeny*, 10(1): 23−46. https://doi.org/10.1127/gtm/2014/0009

Patiño Douce, A. E., 1997. Generation of Metaluminous A-Type Granites by Low-Pressure Melting of Calc-Alkaline Granitoids. *Geology*, 25(8): 743. https://doi.org/10.1130/0091-7613(1997)0250743:gomatg>2.3.co;2

Peccerillo, A., Taylor, S. R., 1976. Geochemistry of Eocene Calc-Alkaline Volcanic Rocks from the Kastamonu Area, Northern Turkey. *Contributions to Mineralogy and Petrology*, 58: 63−81. https://doi.org/10.1007/bf00384745

Pei, F. P., Xu, W. L., Yang, D. B., et al., 2007. Zircon U-Pb Geochronology of Basement Metamorphic Rocks in the Songliao Basin. *Chinese Science Bulletin*, 52: 942−948. https://doi.org/10.1007/s11434-007-0107-2

Prelević, D., Akal, C., Romer, R. L., et al., 2015. Magmatic Response to Slab Tearing: Constraints from the Afyon Alkaline Volcanic Complex, Western Turkey. *Journal of Petrology*, 56(3): 527−562. https://doi.org/10.1093/petrology/egv008

Qian, C., Chen, H. J., Lu, L., et al., 2018. The Discovery of Neoarchean Granite in Longjiang Area, Heilongjiang Province. *Acta Geoscientica Sinica*, 39: 27−36 (in Chinese with English Abstract)

Qian, C., Wang, Y., Lu, L., et al., 2019. Geochronology, Geochemistry and Hf Isotopic Composition of Amphibolite from Zhalantun Region in Northern Great Xing'an Range and Its Tectonic Significance. *Earth Science*, 44(10): 3193−3208 (in Chinese with English Abstract)

Rollinson, H. R., 1993. Using Geochemical Data: Evaluation, Presentation, Interpretation. Longman Singapore Publishers (Pte) Ltd., Singapore. 352

Rosenbaum, G., Gasparon, M., Lucente, F. P., et al., 2008. Kinematics of Slab Tear Faults during Subduction Segmentation and Implications for Italian Magmatism. *Tectonics*, 27(2): TC2008. https://doi.org/10.1029/2007tc002143

Şengör, A. M. C., Natal'In, B. A., Burtman, V. S., 1993. Evolution of the Altaid Tectonic Collage and Palaeozoic Crustal Growth in Eurasia. *Nature*, 364(6435): 299−307. https://doi.org/10.1038/364299a0

She, H. Q., Li, J. W., Xiang, A. P., et al., 2012. U-Pb Ages of the Zircons from Primary Rocks in Middle-Northern Daxinganling and Its Implications to Geotectonic Evolution. *Acta Petrologica Sinica*, 28: 571−594 (in Chinese with English Abstract)

Shi, L., Zheng, C. Q., Yao, W. G., et al., 2015. Geochronological Framework and Tectonic Setting of the Granitic Magmatism in the Chaihe-Moguqi Region, Central Great Xing'an Range, China. *Journal of Asian Earth Sciences*, 113: 443−453. https://doi.org/10.1016/j.jseaes.2014.12.013

Sisson, T. W., Ratajeski, K., Hankins, W. B., et al., 2005. Voluminous Granitic Magmas from Common Basaltic Sources. *Contributions to Mineralogy and Petrology*, 148(6): 635−661. https://doi.org/10.1007/s00410-004-0632-9

Skjerlie, K. P., Johnston, A. D., 1993. Fluid-Absent Melting Behavior of an F-Rich Tonalitic Gneiss at Mid-Crustal Pressures: Implications for the Generation of Anorogenic Granites. *Journal of Petrology*, 34(4): 785−815. https://doi.org/10.1093/petrology/34.4.785

Sun, S. S., McDonough, W. F., 1989. Chemical and Isotopic Systematics of Oceanic Basalts: Implications for Mantle Composition and Processes. *Geological Society, London, Special Publications*, 42(1): 313−345. https://doi.org/10.1144/gsl.sp.1989.042.01.19

Turner, S. P., Foden, J. D., Morrison, R. S., 1992. Derivation of some A-Type Magmas by Fractionation of Basaltic Magma: An Example from the Padthaway Ridge, South Australia. *Lithos*, 28(2): 151−179. https://doi.org/10.1016/0024-4937(92)90029-x

Whalen, J. B., Currie, K. L., Chappell, B. W., 1987. A-Type Granites: Geochemical Characteristics, Discrimination and Petrogenesis. *Contributions to Mineralogy and Petrology*, 95(4): 407−419. https://doi.org/10.1007/bf00402202

Windley, B. F., Alexeiev, D., Xiao, W. J., et al., 2007. Tectonic Models for Accretion of the Central Asian Orogenic Belt. *Journal of the Geological Society*, 164(1): 31−47. https://doi.org/10.1144/0016-76492006-022

Wu, F. Y., Ji, W. Q., Sun, D. H., et al., 2012. Zircon U-Pb Geochronology and Hf Isotopic Compositions of the Mesozoic Granites in Southern Anhui Province, China. *Lithos*, 150: 6−25. https://doi.org/10.1016/j.lithos.2012.03.020

Wu, F. Y., Sun, D. Y., Ge, W. C., et al., 2011. Geochronology of the Phanerozoic Granitoids in Northeastern China. *Journal of Asian Earth Sciences*, 41(1): 1−30. https://doi.org/10.1016/j.jseaes.2010.11.014

Wu, F. Y., Sun, D. Y., Li, H. M., et al., 2001. The Nature of Basement beneath the Songliao Basin in NE China: Geochemical and Isotopic Constraints. *Physics and Chemistry of the Earth, Part A: Solid Earth and Geodesy*, 26(9/10): 793−803. https://doi.org/10.1016/S1464-1895(01)00128-4

Xiao, W. J., Santosh, M., 2014. The Western Central Asian Orogenic Belt: A Window to Accretionary Orogenesis and Continental Growth. *Gondwana Research*, 25(4): 1429−1444. https://doi.org/10.1016/j.

gr.2014.01.008

Xiao, W. J., Song, D. F., Windley, B. F., et al., 2019. Research Progresses of the Accretionary Processes and Metallogenesis of the Central Asian Orogenic Belt. *Science China Earth Sciences*, 49: 1512−1545. https://doi.org/10.1007/s11430-019-9524-6

Xu, B., Charvet, J., Chen, Y., et al., 2013. Middle Paleozoic Convergent Orogenic Belts in Western Inner Mongolia (China): Framework, Kinematics, Geochronology and Implications for Tectonic Evolution of the Central Asian Orogenic Belt. *Gondwana Research*, 23(4): 1342−1364. https://doi.org/10.1016/j.gr.2012.05.015

Xu, B., Zhao, P., Wang, Y. Y., et al., 2015. The Pre-Devonian Tectonic Framework of Xing'an-Mongolia Orogenic Belt (XMOB) in North China. *Journal of Asian Earth Sciences*, 97: 183−196. https://doi.org/10.1016/j.jseaes.2014.07.020

Yang, H., Ge, W. C., Ji, Z., et al., 2019. Late Carboniferous to Early Permian Subduction-Related Intrusive Rocks from the Huolongmen Region in the Xing'an Block, NE China: New Insight into Evolution of the Nenjiang-Heihe Suture. *International Geology Review*, 61(9): 1071−1104. https://doi.org/10.1080/00206814.2018.1493403

Yang, J. H., Wu, F. Y., Shao, J., et al., 2006a. Constraints on the Timing of Uplift of the Yanshan Fold and Thrust Belt, North China. *Earth and Planetary Science Letters*, 246(3/4): 336−352. https://doi.org/10.1016/j.epsl.2006.04.029

Yang, J. H., Wu, F. Y., Chung, S. L., et al., 2006b. A Hybrid Origin for the Qianshan A-Type Granite, Northeast China: Geochemical and Sr-Nd-Hf Isotopic Evidence. *Lithos*, 89(1/2): 89−106. https://doi.org/10.1016/j.lithos.2005.10.002

Yin, J. Y., Chen, W., Xiao, W. J., et al., 2017. Late Silurian−Early Devonian Adakitic Granodiorite, A-Type and I-Type Granites in NW Junggar, NW China: Partial Melting of Mafic Lower Crust and Implications for Slab Roll-back. *Gondwana Research*, 43: 55−73. https://doi.org/10.1016/j.gr.2015.06.016

Zhang, Q., Jin, W. J., Li, C. D., et al., 2010. Revisiting the New Classification of Granitic Rocks based on Whole-Rock Sr and Yb Contents: Index. *Acta Petrologica Sinica*, 26: 985−1015 (in Chinese with English Abstract)

Zhang, Y. J., Zhang, C., Wu, X. W., et al., 2016. Geochronology and Geochemistry of Late Paleozoic Marine Volcanic from the Zhalantun Area in Northern Dahinggan Mountains and Its Geological Significance. *Acta Geologica Sinica*, 90(10): 2706−2720 (in Chinese with English Abstract)

Zhang, Y. Y., Yuan, C., Long, X. P., et al., 2017. Carboniferous Bimodal Volcanic Rocks in the Eastern Tianshan, NW China: Evidence for Arc Rifting. *Gondwana Research*, 43: 92−106. https://doi.org/10.1016/j.gr.2016.02.004

Zhang, Y., Pei, F. P., Wang, Z. W., et al., 2018. Late Paleozoic Tectonic Evolution of the Central Great Xing'an Range, Northeast China: Geochronological and Geochemical Evidence from Igneous Rocks. *Geological Journal*, 53(1): 282−303. https://doi.org/10.1002/gj.2891

Zhao, J. L., Qiu, J. S., Liu, L., et al., 2016. The Late Cretaceous I- and A-Type Granite Association of Southeast China: Implications for the Origin and Evolution of Post-Collisional Extensional Magmatism. *Lithos*, 240/241/242/243: 16−33. https://doi.org/10.1016/j.lithos.2015.10.018

Zhao, X. F., Zhou, M. F., Li, J. W., et al., 2008. Association of Neoproterozoic A- and I-Type Granites in South China: Implications for Generation of A-Type Granites in a Subduction-Related Environment. *Chemical Geology*, 257(1/2): 1−15. https://doi.org/10.1016/j.chemgeo.2008.07.018

Zhao, Z., Chi, X. G., Zhao, X. Y., et al., 2012. LA-ICP-MS U-Pb Geochronology of Detrital Zircon from the Hongshui-Quan Formation in the Northern Da Hinggan Area and Its Tectonic Significance. *Journal of Jilin University* (*Earth Science Edition*), 42(1): 126−135. https://doi.org/10.13278/j.cnki.jjuese.2012.01.031 (in Chinese with English Abstract)

Zhao, Z., Chi, X. G., Liu, J. F., et al., 2010. Late Paleozoic Arc-Related Magmatism in Yakeshi Region, Inner Mongolia: Chronological and Geochemical Evidence. *Acta Petrologica Sinica*, 26(11): 3245−3258 (in Chinese with English Abstract)

Zhou, J. B., Han, J., Zhao, G. C., et al., 2015. The Emplacement Time of the Hegenshan Ophiolite: Constraints from the Unconformably Overlying Paleozoic Strata. *Tectonophysics*, 662: 398−415. https://doi.org/10.1016/j.tecto.2015.03.008

Zhou, J. B., Wilde, S. A., Zhao, G. C., et al., 2018. Nature and Assembly of Microcontinental Blocks within the Paleo-Asian Ocean. *Earth-Science Reviews*, 186: 76−93. https://doi.org/10.1016/j.earscirev.2017.01.012

Zhu, K. Y., Li, Z. X., Xu, X. S., et al., 2016. Early Mesozoic Ferroan (A-Type) and Magnesian Granitoids in Eastern South China: Tracing the Influence of Flat-Slab Subduction at the Western Pacific Margin. *Lithos*, 240/241/242/243: 371−381. https://doi.org/10.1016/j.lithos.2015.11.025